Mon. Not. R. Astron. Soc. **349,** 518–526 (2004) doi:10.1111/j.1365-2966.2004.07515.x

The environments of hyperluminous infrared galaxies at $0.44 < z < 1.55$

D. Farrah,[1⋆] J. Geach,[2,3] M. Fox,[2] S. Serjeant,[4] S. Oliver,[5] A. Verma,[6] A. Kaviani[2] and M. Rowan-Robinson[2]

[1]*SIRTF Science Center, Jet Propulsion Laboratory, California Institute of Technology, Pasadena 91125, USA*
[2]*Astrophysics Group, Blackett Laboratory, Imperial College, Prince Consort Road, London SW7 2BW*
[3]*Astronomy Unit, Queen Mary College, Mile End Road, London E1 4NS*
[4]*Centre for Astrophysics and Planetary Science, School of Physical Sciences, University of Kent, Canterbury, Kent CT2 7NR*
[5]*Astronomy Centre, University of Sussex, Falmer, Brighton BN1 9QJ*
[6]*Max-Planck-Institut fur Extraterrestrische Physik, Postfach 1312, 85741 Garching, Germany*

Accepted 2003 December 4. Received 2003 November 25; in original form 2003 August 14

ABSTRACT

We present deep wide-field K_s-band observations of six Hyperluminous Infrared Galaxies (HLIRGs) spanning a redshift range $0.44 < z < 1.55$. The sample resides in a wide variety of environments, from the field to Abell 2 clusters, with a mean galaxy–HLIRG clustering amplitude of $\langle B_{\rm gh} \rangle = 190 \pm 45$ Mpc$^{1.77}$. The range in environments, and the mean clustering level, are both greater than those seen in local IR-luminous galaxies, from which we infer that the range of galaxy evolution processes driving IR-luminous galaxy evolution at $z > 0.5$ is greater than locally, and includes mergers between gas-rich spiral galaxies in the field, but also includes encounters in clusters and hierarchical build-up. The similarity in the range of environments and mean clustering amplitude between our sample and QSOs over a similar redshift range is consistent with the interpretation where evolutionary connections between IR-luminous galaxies and QSOs are stronger at $z > 0.5$ than locally, and that, at these redshifts, the processes that drive QSO evolution are similar to those that drive IR-luminous galaxy evolution. From comparison of the HLIRG and QSO host galaxies we further postulate that a larger fraction of IR-luminous galaxies pass through an optical QSO stage at $z > 0.5$ than locally.

Key words: galaxies: clusters: general – galaxies: evolution – galaxies: starburst – galaxies: active – infrared: galaxies.

1 INTRODUCTION

Since the discovery by the *Infrared Astronomical Satellite* (*IRAS*) in 1983 of a large population of galaxies with significant infrared (IR) emission, substantial effort has been expended on understanding the nature of the most luminous end of this IR galaxy population. These sources, termed Ultraluminous Infrared Galaxies (ULIRGs) if their IR luminosity exceeds 10^{12} L$_\odot$, and Hyperluminous Infrared Galaxies (HLIRGs) if their IR luminosity exceeds 10^{13} L$_\odot$, are found over a very wide range in redshift, with most lying at $z < 0.1$ (Soifer et al. 1984; Saunders et al. 2000), but with a significant number lying in the range $0.1 < z < 0.4$, and a few lying at higher redshifts. Although the consensus is now that ULIRGs and HLIRGs are powered by some combination of violent star formation and black hole accretion surrounded by large masses of gas and dust, the triggers for this activity, and how these galaxies evolve, are not known. Locally, ULIRGs are thought to be mergers between two or more gas-rich spiral galaxies, taking place almost exclusively in poor environments, and it is thought that a small number of these ULIRGs evolve into optically selected QSOs (Soifer et al. 1984; Leech et al. 1994; Sanders & Mirabel 1996; Rigopoulou et al. 1999; Farrah et al. 2001; Bushouse et al. 2002; Tacconi et al. 2002; Farrah et al. 2003). At higher redshifts, however, the picture is less clear. It has been suggested that a greater variety of galaxy formation processes may play a role amongst ULIRGs and HLIRGs at high redshift (Farrah et al. 2002b), a change which may manifest itself in their environments.

The HLIRGs, which generally lie at $z \geqslant 0.3$, have been studied extensively since their discovery, motivated by their extreme luminosities which make them amongst the most luminous objects in the Universe. The first HLIRG to be found (P09104+4109, at $z = 0.44$) was a cD galaxy in the core of a rich cluster, identified to have extreme IR emission by Kleinmann et al. (1988), with a far-infrared luminosity of $1.5 \times 10^{13} h_{50}^{-2}$ L$_\odot$. Then, in 1991, Rowan-Robinson et al. (1991) identified F10214+4724 at $z = 2.286$, with an apparent far-infrared luminosity of $3 \times 10^{14} h_{50}^{-2}$ L$_\odot$. Later observations revealed a large mass of molecular gas [$10^{11} h_{50}^{-2}$ M$_\odot$ (Brown &

⋆E-mail: duncan@ipac.caltech.edu

Table 1. Hyperluminous infrared galaxy sample.

Name	z	RA (J2000)	Dec	Spectrum	m_{K_s}	L_{ir}	Exp. time (s)	$k_{s,lim}$	$m_{K_s}*$
IRAS F00235+1024	0.58	00 26 06.7	10 41 27.6	nl	17.05	13.15	1521	20.68	16.51
IRAS P09104+4109	0.44	09 13 45.4	40 56 28.0	Sy2	15.00	13.24	2341	20.81	15.90
IRAS F10026+4949	1.12	10 05 52.5	49 34 47.8	Sy1	16.85	14.00	3511	21.02	17.95
IRAS F10119+1429	1.55	10 14 37.8	14 15 59.7	QSO	16.37	∼14.31	3862	20.87	18.69
LBQS 1220+0939	0.68	12 23 17.9	09 23 07.3	QSO	17.54	∼13.08	1170	20.53	16.97
IRAS F14218+3845	1.21	14 23 55.5	38 31 51.3	QSO	17.21	13.26	3277	21.15	18.21

Magnitudes are taken from the data presented in this paper. Infrared ($1 - 1000$ μm) luminosities, given in units of bolometric solar luminosities, are taken from Rowan-Robinson (2000) and Farrah et al. (2002b) and rescaled to $\Lambda = 0.7$, $\Omega_0 = 0.3$ and $H_0 = 70$. $k_{s,\mathrm{lim}}$ is the faintest object detected by SEXTRACTOR for each field. $m^*_{K_s}$ was derived from Pozzetti et al. (2003) for the redshift of each object.

vanden Bout 1991; Solomon, Downes & Radford 1992)], a Seyfert emission spectrum (Elston et al. 1994), and evidence for lensing with a magnification of about 10 in the infrared (Graham & Liu 1995; Broadhurst & Lehar 1995; Eisenhardt et al. 1996; Green & Rowan-Robinson 1996). These objects appeared to presage a new class of infrared galaxy.

Later observations of larger samples of HLIRGs uncovered a more detailed picture. *Hubble Space Telescope* (*HST*) imaging (Farrah et al. 2002a) revealed that a wide range of morphologies are present in the HLIRG population, from merging systems to QSOs in apparently relaxed systems. X-ray, IR, and submillimetre observations showed that, in all cases, HLIRGs are powered by a mixture of dust-enshrouded black hole accretion and violent star formation, with inferred star formation rates of $\geqslant 500\ \mathrm{M}_\odot\ \mathrm{yr}^{-1}$ (Rowan-Robinson 2000; Verma et al. 2002; Farrah et al. 2002b; Wilman et al. 2003), suggesting that HLIRGs are comprised of both mergers between gas-rich spiral galaxies and young galaxies going through their maximal star formation epochs whilst harbouring an AGN.

Despite this progress, the role of HLIRGs in the broader picture of galaxy and active galactic nucleus (AGN) evolution remains unclear. It is not known whether HLIRGs as a class are a simple extrapolation of the local ULIRGs ($L_{\mathrm{ir}} > 10^{12}\ \mathrm{L}_\odot$) making them mostly mergers between gas-rich spirals, or whether a wider range of galaxy formation processes play a role in HLIRG evolution. Also, the links between HLIRGs and QSOs at comparable redshifts are not well understood. Locally, it is thought that some fraction of ULIRGs evolve into optically selected QSOs (Sanders et al. 1988; Farrah et al. 2001; Tacconi et al. 2002), but it is not known whether this is also true in the distant Universe.

Many of these unknowns result from two major obstacles in studying HLIRG evolution. First, HLIRGs contain very large masses of gas and dust, making observations of the galaxies themselves at all wavelengths (except perhaps the far-infrared and submillimetre) prone to obscuration bias. Secondly, the presence of a luminous starburst and AGN in all HLIRGs means that observations will be affected by the orientation of the HLIRG relative to us. These problems can, however, be partly overcome by examining the environments of HLIRGs. Since the determination of environments is independent of orientation and dust content, they are a useful tool in studying AGN evolution, and have been used extensively in studying both normal and active galaxies (Longair & Seldner 1979; Yee & Green 1987; Hill & Lilly 1991; Loveday et al. 1995; Wold et al. 2000; Wold et al. 2001; McLure & Dunlop 2001; Sanchez & Gonzalez-Serrano 2002). Studying the environments of HLIRGs therefore can help to clarify the relations between HLIRGs and other AGN classes.

In this paper, we investigate the environments of six HLIRGs, using deep wide field K_s-band imaging. Observations are described in Section 2 and analysis is described in Section 3. Results are presented in Section 4, with discussion in Section 5. Finally, our conclusions are summarized in Section 6. Unless otherwise stated, we assume $\Lambda = 0.7$, $\Omega_0 = 0.3$ and $H_0 = 70\ \mathrm{km\ s^{-1}\ Mpc^{-1}}$.

2 OBSERVATIONS

We selected for observation six HLIRGs from the sample presented by Rowan-Robinson (2000). The sample, their redshifts and other basic data are presented in Table 1. Five of these objects were selected to lie approximately in the redshift range $0.6 < z < 1.6$, where the greatest evolution in the IR galaxy population is thought to occur (e.g. Rowan-Robinson et al. 1997). Additionally, we observed one further HLIRG, P09104+4109, which lies at $z = 0.44$ and is already known to lie in a rich cluster, to act as a control for our observation and analysis methods, though we do not include this source in the discussion. None of our targets show any evidence for significant gravitational lensing.

Observations were made on 2001 December 25–26 using the INGRID wide-field near-infrared imager and a K_s-band filter, on the 4.2-m William Hershel Telescope (WHT). Isaac Newton Group Red Imaging Device (INGRID) is a 1024×1024 pixel array, with a scale of 0.238 arcsec pixel^{-1}, corresponding to a field of view of ∼17 arcmin^2. At the redshifts of our sample this corresponds to a physical field of view of >1.36 Mpc. The targets were centred approximately in the INGRID field of view, with exposure times selected to reach a minimum depth of $m^*_{K_s} + 2$ at the redshift of each object. Observing conditions were generally good, with little cloud cover and seeing of ∼0.8 arcsec; however, the atmospheric stability was variable, resulting in non-photometric nights. The total exposure time for each object was divided into several nine-point 'box' dither patterns, with a 16.7 arcsec offset between each position, to allow the subtraction of cosmic rays, hot pixels, and the infrared sky background. As the INGRID field of view is too small to reliably estimate field galaxy counts from the edges of the HLIRG fields, separate control fields were also observed, with similar galactic latitudes and exposure times as the sample. For photometric calibration we observed a selection of infrared standard stars throughout each night, at several different airmasses.

3 DATA REDUCTION

Following debiasing and flat-fielding, the data were reduced using our own custom-written IRAF pipeline, based in part on the QUICKLOOK INGRID data reduction pipeline from the Isaac Newton Group (ING). As the exposure time at each position in the dither pattern was only 30 s, particular care was taken in accounting for bright sources when subtracting sky noise. Source masks were created for the

individual frames in each dither pattern by first creating an approximate estimate of the sky by median combining the nine frames in each dither pattern without applying the dither offsets. This 'dummy' sky frame was then subtracted from each frame in the dither pattern to reveal the brightest sources, which were then masked out when creating the 'real' sky frame. The nine frames in each dither pattern were combined using the IRAF task IMCOMBINE, with dither offsets calculated by centroiding two or more bright sources common to each frame. After each dither pattern was combined into a single image, sky subtraction was performed using the 'real' sky frames and pixel masks described earlier. It was found that this sky subtraction method worked well in dealing with variations in the infrared sky between different dither patterns, over the long exposure time for each object. The combined images from each dither pattern were then stacked together to produce a final image I:

$$I = \frac{\sum_i \left(I_i \sigma_i^{-2}\right)}{\sum_i \sigma_i^{-2}}, \tag{1}$$

where I_i and σ_i are the individual images from each dither pattern, and their standard deviations, respectively. The standard deviations were derived from the noise fluctuations in each image. Noisy edges, where the total exposure times were shorter owing to the dither pattern, were clipped off. The resulting field of view, at 13×13 arcmin^2, was still sufficient to quantify the environments of the sample. The final images were of excellent quality, and flat to better than 1 per cent across the width of the frame, and were in all cases of much higher quality than the images from the QUICKLOOK reduction. Our reduction pipeline, INREP, is available for general use via the Isaac Newton Group (ING) web pages.[1]

Sources were extracted and catalogued using the SEXTRACTOR package (Bertin & Arnouts 1996). For source extraction, we adopted the conservative criterion that a source constitutes at least four contiguous pixels, with a significance of detection of at least 3σ above the background. The default SEXTRACTOR extraction filter was used to detect faint extended objects, with 32 deblending thresholds, a cleaning efficiency of 1 and a contrast parameter of 0.005. The background estimation was mesh based, with a mesh size of 64 and a filter size of 3. As many of the sources in the frames were faint and slightly extended, the magnitudes were calculated using corrected isophotal (ISOCOR) magnitudes within SEXTRACTOR. The calibration zero-point magnitudes for each object frame and control frame were calculated using the observations of the infrared standard stars. The errors on the final magnitudes arising from the standard star calibrations are $\Delta\, m = 0.05$, with a further error of $\Delta\, m = 0.05$ from the source extraction. To correct our measured magnitudes to the rest-frame K_s band, we computed k-corrections assuming a standard power law, with $\alpha = 2$.

4 ANALYSIS

To evaluate the environmental richness of each object in our sample we use two independent clustering measures: the $B_{\rm gg}$ galaxy–galaxy correlation statistic (Longair & Seldner 1979), which for our sample we refer to as the $B_{\rm gh}$ galaxy–HLIRG correlation statistic, and the $N_{0.5}$ statistic (Hill & Lilly 1991). The $B_{\rm gh}$ statistic is the amplitude of the spatial cross-correlation function, and relies on knowing the volume density of galaxies around the HLIRG, which itself requires knowledge of the luminosity function (LF). The $N_{0.5}$ statistic is a simple, more direct counting statistic, and involves counting all the sources within 0.5 Mpc of the target that lie within a certain magnitude range. Although the $B_{\rm gh}$ statistic is physically more meaningful than the $N_{0.5}$ statistic, the near-infrared luminosity function is not known with great precision at high redshifts. Therefore, we have adopted the $B_{\rm gh}$ statistic as our primary measure of environmental richness, but we also use the $N_{0.5}$ statistic as an independent check.

To compute the $B_{\rm gh}$ statistic, we follow the prescription of Longair & Seldner (1979). As this statistic is not trivial to evaluate, we provide a detailed outline of the procedure here. The spatial cross-correlation function, $\xi(r)$, can be described as a simple power law:

$$\xi(r) = B_{\rm gh} r^{-\gamma}, \tag{2}$$

and is derived from the galaxy–HLIRG angular cross-correlation function $w(\theta)$,

$$w(\theta) = A_{\rm gh} \theta^{1-\gamma}, \tag{3}$$

by deprojecting from the celestial sphere. The amplitude of the angular cross-correlation function, $A_{\rm gh}$, is essentially the richness measure of the number of galaxies about a point on the sky, and is converted to $B_{\rm gh}$, the richness measure of the number of galaxies about a point in *space*, by translating the angular cross-correlation function $w(\theta)$ to the spatial cross-correlation function $\xi(r)$.

To perform this conversion, the $A_{\rm gh}$ statistic is evaluated:

$$A_{\rm gh} = \frac{N_T - N_B}{N_B} \frac{3-\gamma}{2} \theta^{\gamma-1}. \tag{4}$$

where N_T is the total number of galaxies within a radius θ around the target, corresponding to 0.5 Mpc at the target redshift, and N_B is the number of galaxies within the same radius in the control field for that object. We make the assumption (Wold et al. 2000; Wold et al. 2001) that $\gamma = 1.77$. The precise choice of γ will, however, not affect the derived clustering amplitudes, as it has previously been shown (Prestage & Peacock 1988; Prestage & Peacock 1989) that $B_{\rm gh}$ is insensitive to the choice of γ, as long as $\gamma \sim 2$.

The $B_{\rm gh}$ statistic can now be calculated, and normalized to the integral LF, $\Phi(m_l, z)$ which represents the number of galaxies more luminous than m_l per unit comoving volume at redshift z:

$$B_{\rm gh} = \frac{\rho_{\rm g} A_{\rm gh}}{\Phi(m_l, z) I_\gamma} d_\theta^{\gamma-3}, \tag{5}$$

where $\rho_{\rm g}$ is the average surface density of background galaxies, d_θ is the angular diameter distance to the target and I_γ is an integration constant:

$$I_\gamma = \frac{2^\gamma}{\gamma - 1} \frac{\Gamma^2[(\gamma+1)/2]}{\Gamma(\gamma)} \sim 3.78. \tag{6}$$

The integration to $\Phi(m_l, z)$ is performed by taking a universal LF of the form (Schechter 1976)

$$\phi(L) \sim (\phi^*/L^*)(L/L^*)^\alpha \exp(-L/L^*) \tag{7}$$

and integrating down to the completeness limit at the target redshift $L(m_l, z)$:

$$\Phi(m_l, z) = \int_{L(m_l,z)}^{\infty} \phi(L) {\rm d}L. \tag{8}$$

For the parameters used in the LF, we use the most recent determination of the high redshift near-IR LFs as given by Pozzetti et al. (2003), who have determined the evolution of the near-IR LF in the J- and K_s bands in redshift bins of $z = \langle\, 0.20, 0.65 \rangle$ and $z = \langle\, 0.75, 1.30 \rangle$, using a spectroscopic survey of a magnitude-limited sample of galaxies with $K_s < 20$. In terms of absolute magnitudes the luminosity function can be expressed as

$$\phi(M) = C f(M)^{(\alpha+1)} \exp[-f(M)] \tag{9}$$

[1] http://ing.iac.es/Astronomy/Ingrid

where the constant $C = 0.4 \ln(10)\phi^*$, and

$$f(M) = 10^{-0.4(M-M^*)}. \quad (10)$$

As some of the galaxies in our sample lie outside the redshift bins given by Pozzetti et al. (2003), we must make assumptions as to the nature of the LF at these magnitudes. In the redshift range $0.2 < z < 0.65$, we have assumed $\alpha = -1.25$, $M^* = -25.64$ and $\phi^* = 6.11 \times 10^{-4}$ Mpc^{-3}. In the redshift range $0.75 < z < 1.55$ we have assumed $\alpha = -0.98$, $M^* = -25.54$ and $\phi^* = 9.98 \times 10^{-4}$ Mpc^{-3}. We note that Pozzetti et al. (2003) find only mild evolution in the K_s-band luminosity function over the redshift range $0 < z < 1.3$, hence our use of their luminosity function at $z = 1.55$ is unlikely to be a major source of error.

The errors in $A_{\rm gh}$ and $B_{\rm gh}$ were calculated following the prescription given by Yee & Lopez-Cruz (1999):

$$\frac{\Delta A_{\rm gh}}{A_{\rm gh}} = \frac{\Delta B_{\rm gh}}{B_{\rm gh}} = \frac{\sqrt{(N_T - N_B) + 1.3^2 N_B}}{N_T - N_B}, \quad (11)$$

which is based only upon (non-Poissonian) counting statistics. Other systematic errors are discussed in Section 5.2.

To compute the $N_{0.5}$ statistic, we follow the procedure described by Hill & Lilly (1991). This statistic is computed by counting all sources within a 0.5 Mpc radius of the target, with a magnitude in the interval $\langle m, m+3\rangle$, where m is the magnitude of the target. Subtracted from this number is the expected number of background field galaxies in the same magnitude interval calculated from the control fields. The resulting number is the $N_{0.5}$ statistic. This measurement does not require integration of a luminosity function, although if the luminosities of HLIRGs and cluster galaxies evolve very differently with redshift then the $N_{0.5}$ statistic will give inaccurate results. There is no evidence why this should be a major effect however, so we do not take it into account. From Table 1, the limiting magnitude for each object is fainter than $m_{\rm HLIRG} + 3$ except for two cases: the image for F10119+1429 reaches $m_{\rm HLIRG} + 2.18$, and the image for F14218+3845 reaches $m_{\rm HLIRG} + 2.94$. In both these cases, however, the limiting depth is sufficiently near $m_{\rm HLIRG} + 3$ that the $N_{0.5}$ statistic is still usable.

5 RESULTS

5.1 Clustering statistics

Images of the fields around each HLIRG are presented in Fig. 1. In Fig. 2 we plot the galaxy counts in a 0.5 Mpc region around each HLIRG, and the counts for the associated control field. The $B_{\rm gh}$ and $N_{0.5}$ statistics for each object, and their errors, are given in Table 2. We also quote the approximate Abell classes of our sample in this table, based on the conversions given by Hill & Lilly (1991), in our cosmology. We note, however, that these conversions are arbitrary, and hence we base our quoted Abell classes on both the $B_{\rm gh}$ and $N_{0.5}$ statistics.

A wide variety of environments can be seen amongst the objects in the sample. P09104+4109 resides in an Abell 2 cluster, in agreement with previous results (Hines & Wills 1993). For the remaining objects, three reside in poor environments, and two, F10026+4949 and F10119+1429, reside in clusters, of Abell class 1 and 0 respectively, though we note that the detection of clustering for F10119+1429 is marginal, at $\sim 2.5\sigma$. Excluding P09104+4109, the error weighted mean clustering amplitude for the remaining five objects is $\langle B_{\rm gh}\rangle = 190 \pm 45$ Mpc$^{1.77}$.

We can compare the values of $N_{0.5}$ and $B_{\rm gh}$ to each other, as these quantities have been used by many previous authors, and a well defined relation has been found between them. Hill & Lilly (1991) derive $B_{\rm gh} \propto 30 N_{0.5}$. In Fig. 3 we plot this relation, together with $B_{\rm gh}$ versus $N_{0.5}$ for the objects in our sample, and the conversions between $B_{\rm gh}$ and Abell class given by Hill & Lilly (1991). We also plot the best-fitting linear relation between $B_{\rm gh}$ and $N_{0.5}$ for our data. The best fit is well matched to the relation derived by Hill & Lilly (1991) and the objects in the sample follow this relation closely; hence we conclude that our computed values of $N_{0.5}$ and $B_{\rm gh}$ are reasonable.

5.2 Error budget

The errors quoted in Table 2 for the $B_{\rm gh}$ and $N_{0.5}$ statistics are only the counting errors, and do not include three further potentially important sources of error. In this section, we discuss these three error sources in turn.

The first of these is the luminosity function assumed in calculating the $B_{\rm gh}$ statistic. Owing to the uncertainties in the high redshift K_s-band LF used in this paper, this is an important issue to address. Yee & Lopez-Cruz (1999) have examined the sensitivity of $B_{\rm gh}$ to the form of the LF, and find that an error in the assumed value of M^* of up to ± 0.5 mag will still yield essentially the same results. Similarly, an error in α of up to $\pm$ 0.3 will only affect $B_{\rm gh}$ by at most $\sim$20 per cent. Although the K-band LF is not well constrained at the redshifts of our targets, we do not expect that the true LF differs from our assumed LF by such gross margins, and therefore we conclude that uncertainties in our computed $B_{\rm gh}$ statistics owing to the assumed LF are at most 10 per cent.

The second of these error sources is the method used to compare the data to the luminosity function in calculating the $B_{\rm gh}$ statistic. This can be done in two ways. The data can be k-corrected to the rest-frame K_s band, and compared with the K_s-band luminosity function given by Pozzetti et al. (2003), or the data can be compared directly with the J band luminosity function presented by Pozzetti et al. (2003), without applying a k-correction, as the

Table 2. HLIRG clustering statistics.

Name	$N_{0.5}$	$\sigma_{N_{0.5}}$	$A_{\rm gh}$ $\times 10^3$ rad$^{0.77}$	$\sigma_{A_{\rm gh}}$	$B_{\rm gh}$ Mpc$^{1.77}$	$\sigma_{B_{\rm gh}}$	Abell class
IRAS F00235+1024	7.69	2.77	0.66	0.28	208.63	88.31	field
IRAS P09104+4109	29.65	5.45	2.75	0.40	819.75	119.77	2
IRAS F10026+4949	17.81	4.22	1.73	0.40	611.46	141.01	1
IRAS F10119+1429	8.88	2.98	0.72	0.31	384.32	167.33	0
LBQS 1220+0939	3.77	1.94	0.40	0.26	143.78	94.25	field
IRAS F14218+3845	4.45	2.11	0.06	0.21	21.84	81.27	field

Quoted errors only include the counting errors. The methods used to calculate the $B_{\rm gh}$ and $N_{0.5}$ statistics, and the Abell classes, are described in Sections 4 and 5 respectively.

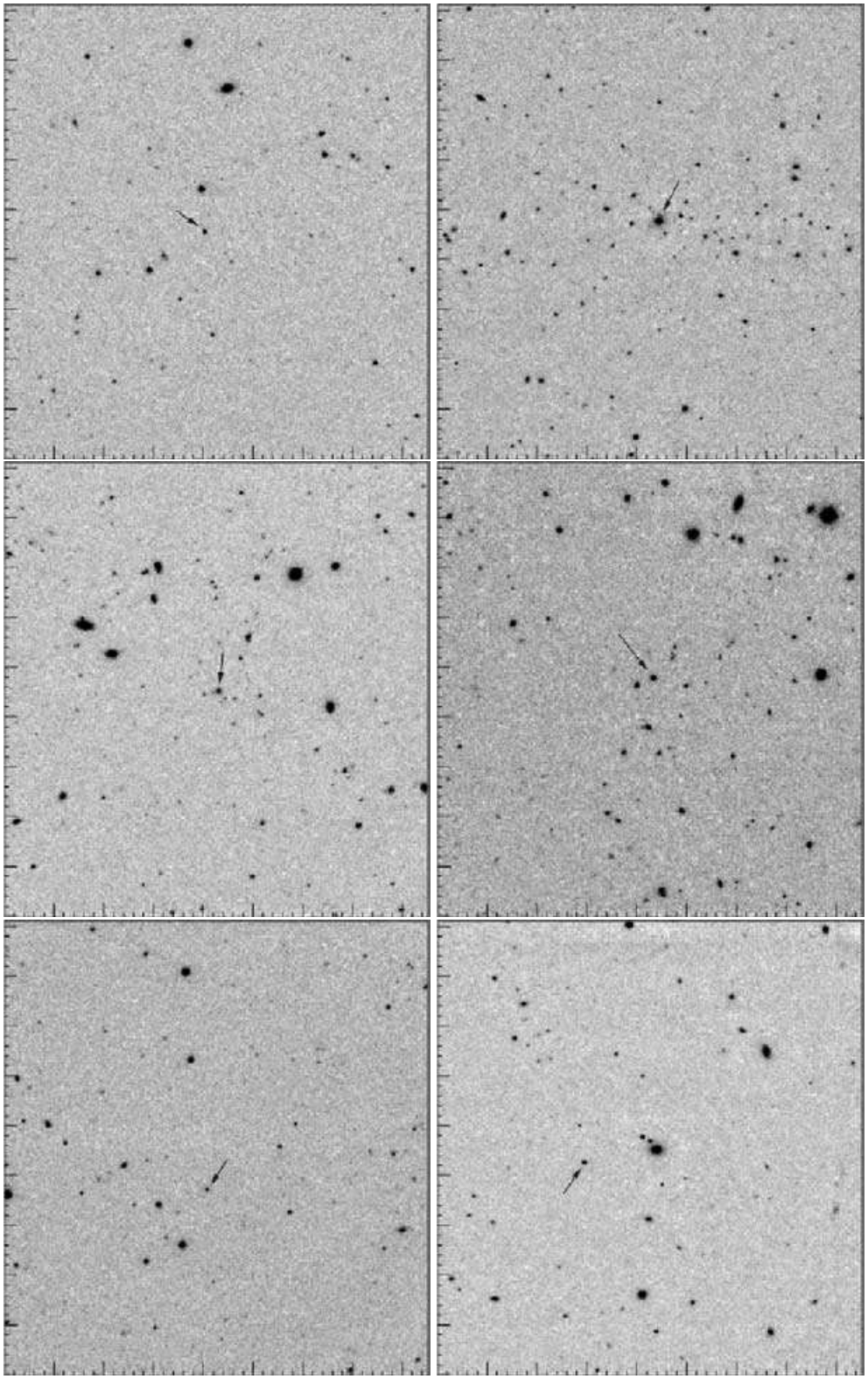

Figure 1. K_s-band images of the fields around each HLIRG. An arrow indicates the HLIRG. Large tick marks correspond to 25″. L–R: (top row) F00235+1024 and P09104+4109, (middle row) F10026+4949 and F10119+1429, (bottom row) LBQS1220+0939 and F14218+3845.

observed frame K_s band approximately the samples rest-frame J band at the redshifts of our sample. Both methods have advantages and disadvantages; the rest-frame K_s band is a less contaminated tracer of evolved stellar mass than the J band, but suffers from the extra uncertainties introduced by applying k-corrections. Although we chose to k-correct our data to the rest-frame K_s band, we also examined the effect of comparing our data directly to the rest-frame J-band luminosity function, without applying k-corrections. We

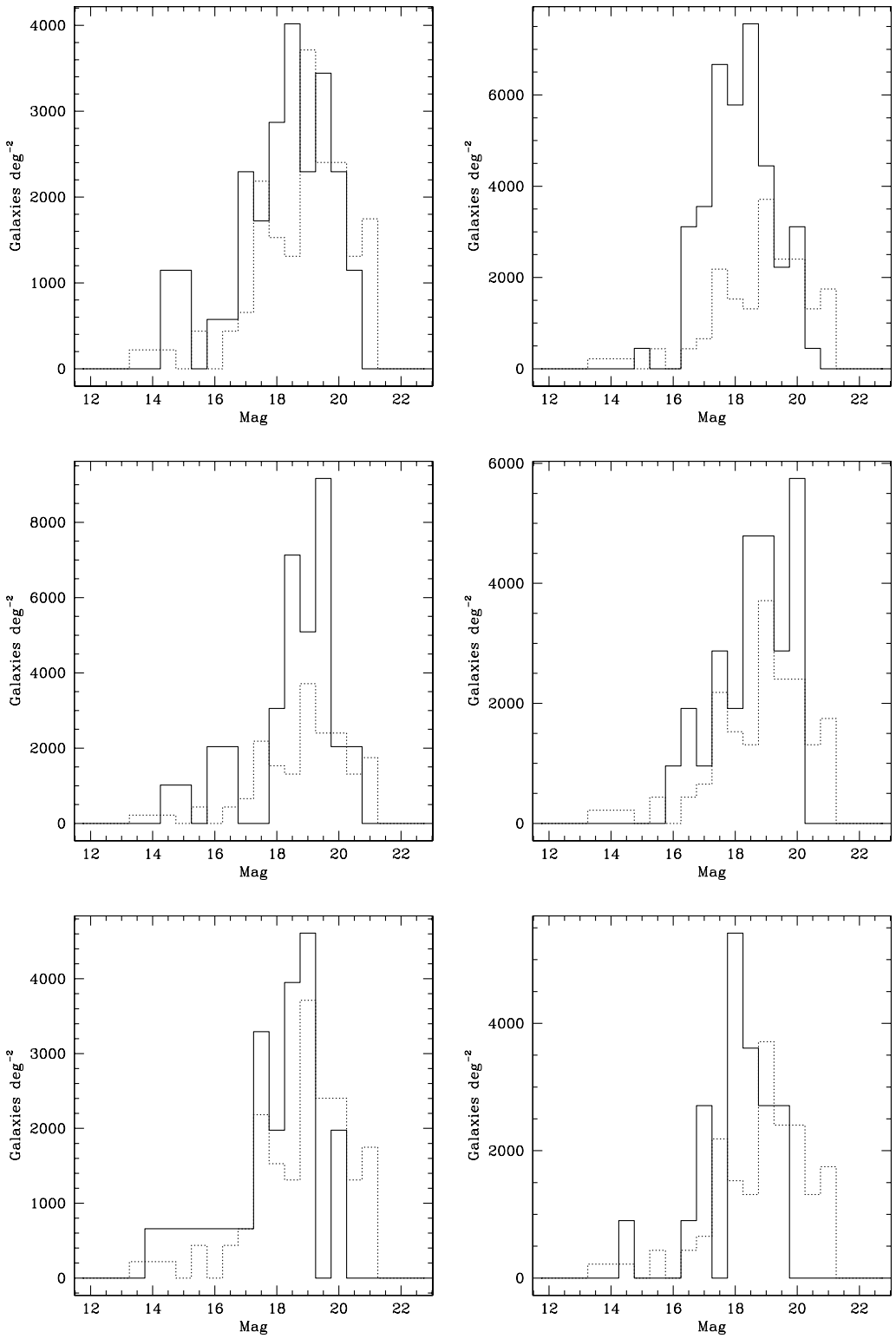

Figure 2. Galaxy counts in a circular region 0.5 Mpc in radius around each HLIRG. The solid line shows the counts in the field around the HLIRG, and the dashed line shows the counts in the control field. L–R: (top row) F00235+1024 and P09104+4109, (middle row) F10026+4949 and F10119+1429, (bottom row) LBQS1220+0939 and F14218+3845. Error bars have been omitted for clarity.

computed $B_{\rm gh}$ and $\sigma_{B_{\rm gh}}$ without applying k-corrections, and using the J-band luminosity function from Pozzetti et al. (2003), and found that the $B_{\rm gh}$ values were within 1σ of the values computed using k-corrections and the K_s-band luminosity function for all the objects except F10119+1429, which was within 1.5σ. Furthermore, each object still resided within the same type of environment as before, with P09104+4109, F10026+4949 and F10119+1429 residing in clusters (with the same significance of detection of clustering) and

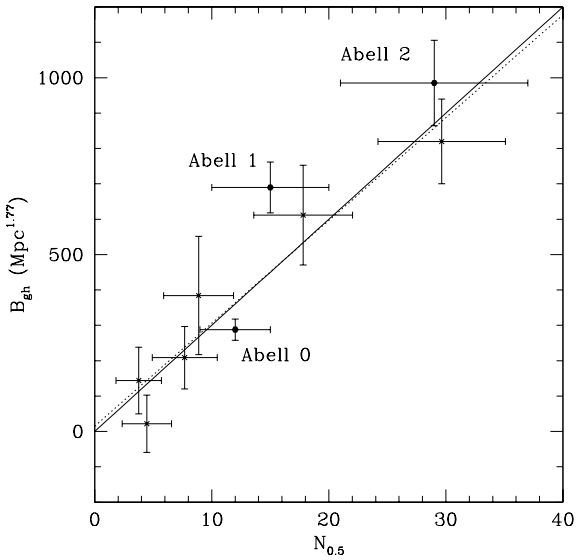

Figure 3. $B_{\rm gh}$ versus $N_{0.5}$ for our sample. Filled hexagons are the Abell calibrations taken from Hill & Lilly (1991), stars are our data. The solid line shows the relation $B_{\rm gh} \propto 30 N_{0.5}$ found by Hill & Lilly (1991). The dashed line is a least squares fit of our data, which gives $B_{\rm gh} = 29.07 N_{0.5} + 14.95$

the other three objects lying in the field. The values of $B_{\rm gh}$ and $\sigma_{B_{\rm gh}}$ were however in all cases slightly higher using the J-band luminosity function and no k-corrections, with F10026+4949 and F10119+1429 predicted to (just) lie in Abell 2 clusters. We conclude that using the K_s-band luminosity function with k-corrections, or just the J-band luminosity function, will not significantly change our results, and that our choice of using the K_s-band luminosity function with k-corrections was the most conservative.

The third of these error sources is the choice of cosmology. Whilst both $B_{\rm gh}$ and $N_{0.5}$ are *relatively* insensitive to the choice of Λ and Ω_0, the sensitivity to H_0 is marked, particularly in the range $65 < H_0 < 80$. This is illustrated in Fig. 4, where we have plotted $B_{\rm gh}$ as a function of H_0 for F10026+4949. By varying H_0 over a relatively small range, the effect on $B_{\rm gh}$ is dramatic, changing from $B_{\rm gh} \sim 350$

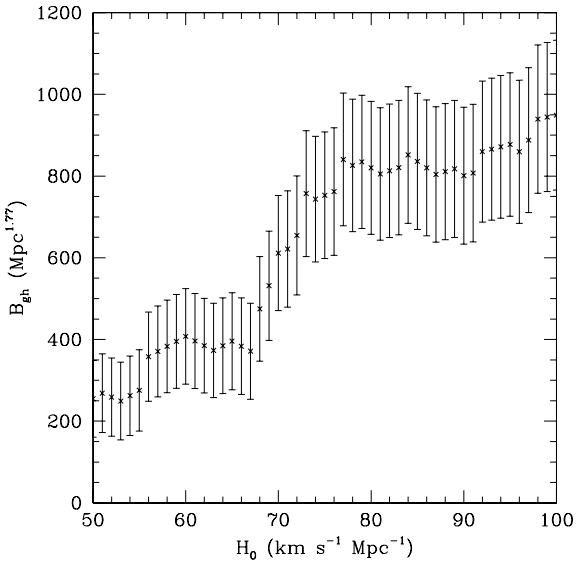

Figure 4. The clustering amplitude of F10026+4949 as a function of H_0 (for $\Lambda = 0.7$, $\Omega_0 = 0.3$). Error bars are the Poisson errors.

for $H_0 = 65$ to $B_{\rm gh} \sim 800$ for $H_0 \geqslant 75$. Most current measurements of H_0 produce values in the range 70 to 75, albeit with a significant error (Freedman et al. (2001) and references therein). Our adopted value of $H_0 = 70$, and therefore our derived clustering amplitudes, are therefore conservative.

In summary, we conclude that, whilst there are further, significant sources of error than the Poisson errors on the derived clustering statistics, none of these sources of error should significantly change our results. Furthermore, we have in all cases adopted the most conservative method possible in computing the clustering amplitudes, making it highly unlikely that any of our objects that we infer to lie in clusters actually reside in the field.

6 DISCUSSION

6.1 The hyperluminous phenomenon at low and high redshift

Our sample of five objects (excluding P09104), although small, exhibits a wide variety of environments, from poor environments to Abell $\sim$1 clusters. This strongly suggests that there is a wide variety of environments amongst objects with high levels of IR emission at $z \sim 1$ generally, although a larger sample would be required to confirm this. This variety of environments is not seen amongst local ULIRGs, which are generally not found in rich environments (Sanders & Mirabel 1996). The mean environmental richness of our sample, at $\langle B_{\rm gh} \rangle = 190 \pm 45$ Mpc$^{1.77}$, is higher, at just over 3σ significance, than the galaxy–galaxy correlation statistic both locally (Loveday et al. 1995; Guzzo et al. 1997) and at moderate redshifts (Hudon & Lilly 1996), though we note that the latter study measured values of $B_{\rm gg}$ up to redshifts of only $z \sim 0.5$. We infer that, in going from $z \sim 0$ to $z \sim 1$ the environments of IR-luminous galaxies become more diverse, and that the mean environment becomes richer than that of normal galaxies both locally and at moderate redshifts. This is supportive of the idea that a wider variety of galaxy formation processes are important amongst the IR-luminous galaxy population at high redshift than locally, such as hierarchical build-up or encounters in clusters. Indeed, one object in our sample, IRAS F10026+4949, may be an example of such a galaxy. This source harbours both a starburst and an AGN (Farrah et al. 2002b), and lies in a rich cluster. From *HST* imaging, this source also possesses multiple very close companions (Farrah et al. 2002a). It is thus an excellent candidate for being a cD galaxy in the process of formation in a cluster at $z = 1.12$, and may be the higher redshift analogue of the clustered IR-luminous active galaxies P09104+4109 and P18216+6419 (Schneider et al. 1992; Hines & Wills 1993; Wold et al. 2002).

6.2 Comparison with quasar environments

Since environments are independent of orientation, we can compare the environments of our sample to those of other classes of active galaxies at comparable redshifts to examine possible relationships between HLIRGs and other AGN classes. The environments of AGN over a wide redshift range have been studied by many authors in efforts to disentangle the myriad AGN taxonomy. Radio-loud QSOs (RLQs) and radio galaxies (RGs) are found in a diverse range of environments, from the field to Abell Class 2 and greater, at both low and high redshift (Longair & Seldner 1979; Yee & Green 1987; Prestage & Peacock 1988; Prestage & Peacock 1989; Hill & Lilly 1991; Allington-Smith et al. 1993; Zirbel 1997; Wold et al. 2000; Sanchez & Gonzalez-Serrano 2002). Overall, RLQs and RGs appear to prefer moderately rich environments on average, of around

Abell Class 0. Determining whether or not there is evolution in the environments of RLQs or RGs with redshift is difficult, owing to gravitational lensing and selection biases, but from recent results it appears that there is no significant difference in RLQ and RG environments at $z < 1.0$ (Wold et al. 2000). For radio-quiet Quasars (RQQs) a broadly comparable picture has now emerged. RQQs are found in a similarly diverse range of environments to RLQs, from the field to Abell class 2 or richer, over a wide redshift range (Yee & Green 1987; Dunlop et al. 1993; Fisher et al. 1996; Deltorn et al. 1997; Tanaka et al. 2000; McLure & Dunlop 2001). Indeed, the most recent results, based on deep optical imaging, show that the environments of RQQs and RLQs at moderate redshifts are statistically indistinguishable (Wold et al. 2001). At $z \geqslant 1$ there is as yet no clear consensus, but the environments of RLQs and RQQs at these redshifts do not appear to be significantly different (Hintzen, Romanishin & Valdes 1991; Hutchings, Crampton & Johnson 1995; Hutchings 1995).

In the local Universe, it was initially suggested that ULIRGs as a class are precursors to optically selected QSOs, although later results show that this is probably true for only a small subset of the ULIRG population (Sanders et al. 1988; Farrah et al. 2001; Tacconi et al. 2002). This is reflected in their environments, as locally ULIRGs and QSOs reside in different environments, with ULIRGs generally lying in the field and QSOs lying in moderately rich environments on average, with a diverse range. We can compare the range of environments in our sample of HLIRGs with those of QSOs at comparable redshifts to see if this is also true at high redshift. The diverse range of environments seen in our sample of HLIRGs is qualitatively similar to the range seen in RLQs and RQQs, and our mean value for $B_{\rm gh}$ is comparable to the mean galaxy–quasar correlation statistic, $B_{\rm gq}$, for RLQs and RQQs at similar redshifts (Wold et al. 2000; Wold et al. 2001). This is illustrated in Fig. 5, where we plot clustering amplitudes versus redshifts for our HLIRGs, together with a representative sample of clustering amplitudes for QSOs from the literature (Yee & Ellingson 1993; Hall & Green 1998; Wold et al. 2000; Wold et al. 2001), converted to our cosmology. The error bars on the QSOs have been intentionally omitted for clarity, but are comparable in size to the error bars on the HLIRGs. We note that the clustering measures were derived using different data, with our clustering amplitudes derived from K_s-band data and the clustering amplitudes from the other samples derived from multiband optical data; however, it is unlikely that this will introduce any systematic biases between the data sets. Therefore, we extrapolate from this that evolutionary links between IR-luminous galaxies and optically selected QSOs may become stronger with increasing redshift. Furthermore, we postulate that, at approximately $z > 0.5$, the range of galaxy evolution processes driving IR-luminous galaxy evolution caused by the greater diversity in environments is similar to the range driving QSO evolution. We note that one object in our sample, LBQS 1220+0939, is a QSO from the Large Bright Quasar Survey (Hewett, Foltz & Chaffee 1995) that was only later discovered to be hyperluminous in the IR; the selection criteria for this object therefore make it unsuitable for determining evolutionary connections between HLIRGs and QSOs. Even with LBQS 1220+0939 removed, however, the sample still contains the same diverse range of environments, and the mean clustering amplitude is still comparable to that of QSOs at similar redshifts.

We can take this one step further via a comparison of HLIRG and optically selected QSO host galaxies. QSOs at all redshifts are thought to lie in luminous, $>L^*$ host galaxies, with elliptical hosts becoming more prevalent for both RLQs and RQQs with increasing optical nuclear luminosity (McLure et al. 1999; Percival et al. 2001; Dunlop et al. 2003). Conversely, although local ULIRGs are thought to evolve into ellipticals with a few also passing though a QSO phase, there are thought to be mergers between (optically) sub-L^* galaxies, with the majority of ULIRGs themselves also being sub-L^* (Colina et al. 2001). For the HLIRGs in our sample, this is not the case. One object, F14218+3845, is a QSO with a host magnitude that suggests (similarly to the other QSOs in the sample) the host is a very luminous, massive system (Farrah et al. 2002a). For the two non-QSOs in our sample, the picture is less clear, with one object (F00235+1024) being 0.5 magnitudes dimmer than m_K^*, but the other (F10026+4949) over a magnitude brighter than m_K^*. We note, however, that the I-band magnitudes of those HLIRGs without a QSO presented by Farrah et al. (2002a) are, with the exception of F00235+1024, much brighter than m_I^*. Whilst more data is evidently needed, it appears reasonable to assume that IR-luminous galaxies may become more similar to QSO hosts with increasing redshift. Whilst this reinforces the idea that evolutionary links between IR-luminous galaxies and QSOs become stronger with increasing lookback time, it also suggests that, at $z \geqslant 0.5$, a greater number of IR-luminous galaxies evolve directly into optically selected QSOs than locally.

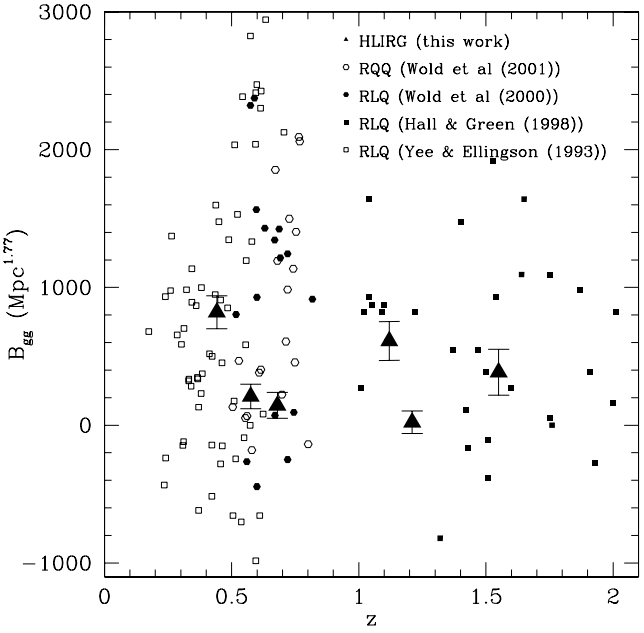

Figure 5. The clustering amplitude versus redshift for the HLIRGs in our sample. Also plotted are clustering amplitudes for QSOs taken from Yee & Ellingson (1993), Hall & Green (1998), Wold et al. (2000) and Wold et al. (2001), converted to our cosmology. The HLIRGs are plotted as larger symbols for clarity.

7 CONCLUSIONS

We have presented deep wide-field K-band imaging of the fields of six hyperluminous infared galaxies, and quantified their environments using the $B_{\rm gh}$ galaxy–HLIRG correlation amplitude, and the $N_{0.5}$ clustering statistic. We conclude the following.

(1) The HLIRGs in our sample reside in a diverse range of environments, from the field to Abell 2 clusters. The mean clustering level of the sample, at $\langle B_{\rm gh} \rangle = 190 \pm 45$, and the range of environments, are both significantly greater than those of the most luminous IR galaxies locally. We infer that, at high redshift, the galaxy evo-

lution processes driving the evolution of IR-luminous galaxies are more diverse than at low redshift, and include mergers between gas-rich spirals in the field, but also include encounters in clusters and hierarchical build-up.

(2) The mean clustering amplitude of the sample, and the range in environments, are comparable to those of QSOs over a similar redshift range. We postulate from this that, at $z \geqslant 0.5$, the range of galaxy evolution processes driving IR-luminous galaxy evolution is similar to the range that drives QSO evolution. When combined with the similarities between HLIRG host galaxies and QSO host galaxies at the same redshifts, this further suggests that a greater fraction of IR-luminous galaxies evolve directly into optically selected QSOs at high redshift than do locally.

ACKNOWLEDGMENTS

We thank Carol Lonsdale and Margrethe Wold for illuminating discussion, and the referee for a very helpful report. This paper is based on observations made with the William Herschel Telescope operated on the island of La Palma by the Isaac Newton Group in the Spanish Observatorio del Roque de los Muchachos of the Instituto de Astrofisica de Canarias. This research has made use of the NASA/IPAC extragalactic database (NED) which is operated by the Jet Propulsion Laboratory, California Institute of Technology, under contract with the National Aeronautics and Space Administration.DF was supported by NASA grant NAG 5-3370 and by the Jet Propulsion Laboratory, California Institute of Technology, under contract with NASA. MF and AK were supported by PPARC.

REFERENCES

Allington-Smith J. R., Ellis R., Zirbel E. L., Oemler A., 1993, ApJ, 404, 521
Bertin E., Arnouts S., 1996, A&AS, 117, 393
Broadhurst T., Lehar J., 1995, ApJ, 450, L41
Brown R. L., vanden Bout P. A., 1991, AJ, 102, 1956
Bushouse H. A. et al., 2002, ApJS, 138, 1
Colina L. et al., 2001, ApJ, 563, 546
Deltorn J.-M., Le Fevre O., Crampton D., Dickinson M., 1997, ApJ, 483, L21
Dunlop J. S., Taylor G. L., Hughes D. H., Robson E. I., 1993, MNRAS, 264, 455
Dunlop J. S., McLure R. J., Kukula M. J., Baum S. A., O'Dea C. P., Hughes D. H., 2003, MNRAS, 340, 1095
Eisenhardt P. R., Armus L., Hogg D. W., Soifer B. T., Neugebauer G., Werner M. W., 1996, ApJ, 461, 72
Elston R., McCarthy P. J., Eisenhardt P., Dickinson M., Spinrad H., Januzzi B. T., Maloney P., 1994, AJ, 107, 910
Farrah D. et al., 2001, MNRAS, 326, 1333
Farrah D., Verma A., Oliver S., Rowan-Robinson M., McMahon R., 2002a, MNRAS, 329, 605
Farrah D., Serjeant S., Efstathiou A., Rowan-Robinson M., Verma A., 2002b, MNRAS, 335, 1163
Farrah D., Afonso J., Efstathiou A., Rowan-Robinson M., Fox M., Clements D., 2003, MNRAS, 343, 585
Fisher K. B., Bahcall J N., Kirhakos S., Schneider D. P., 1996, ApJ, 468, 469
Freedman W. et al., 2001, ApJ, 553, 47
Graham J. R., Liu M. C., 1995, ApJ, 449, L29
Green S. M., Rowan-Robinson M., 1996, MNRAS, 279, 884
Guzzo L., Strauss M. A., Fisher K. B., Giovanelli R., Haynes M. P., 1997, ApJ, 489, 37
Hall P. B., Green R. F., 1998, ApJ, 507, 558
Hewett P. C., Foltz C. B., Chaffee F. H., 1995, AJ, 109, 1498
Hill G. J., Lilly S. J., 1991, ApJ, 367, 1
Hines D. C., Wills B. J., 1993, ApJ, 415, 82
Hintzen P., Romanishin W., Valdes F., 1991, ApJ, 366, 7
Hudon J. D., Lilly S. J., 1996, ApJ, 469, 519
Hutchings J. B., Crampton D., Johnson A., 1995, AJ, 109, 73
Hutchings J. B., 1995, AJ, 109, 928
Kleinmann S. G., Hamilton D., Keel W. C., Wynn-Williams C. G., Eales S. A., Becklin E. E., Kuntz K. D., 1988, ApJ, 328, 161
Leech K. J., Rowan-Robinson M., Lawrence A., Hughes J. D., 1994, MNRAS, 267, 253
Longair M. S., Seldner M., 1979, MNRAS, 189, 433
Loveday J., Maddox S. J., Efstathiou G., Peterson B. A., 1995, ApJ, 442, 457
McLure R. J., Kukula M. J., Dunlop J. S., Baum S. A., O'Dea C. P., Hughes D. H., 1999, MNRAS, 308, 377
McLure R. J., Dunlop J. S., 2001, MNRAS, 321, 515
Percival W. J., Miller L., McLure R. J., Dunlop J. S., 2001, MNRAS, 322, 843
Pozzetti L. et al., 2003, A&A, 402, 837
Prestage R. M., Peacock J. A., 1988, MNRAS, 230, 131
Prestage R. M., Peacock J. A., 1989, MNRAS, 236, 959
Rigopoulou D., Spoon H. W. W., Genzel R., Lutz D., Moorwood A. F. M., Tran Q. D., 1999, AJ, 118, 2625
Rowan-Robinson M., 2000, MNRAS, 316, 885
Rowan-Robinson M. et al., 1991, Nat, 351, 719
Rowan-Robinson M. et al., 1997, MNRAS, 289, 490
Sanchez S. F., Gonzalez-Serrano J. I., 2002, A&A, 396, 773
Sanders D. B., Soifer B. T., Elias J. H., Madore B. F., Matthews, K., Neugebauer G., Scoville N. Z., 1988, ApJ, 325, 74
Sanders D. B., Mirabel I. F., 1996, ARA&A, 34, 749
Saunders W. et al., 2000, MNRAS, 317, 55
Schechter P., 1976, ApJ, 203, 297
Schneider D. P., Bahcall J. N., Gunn J. E., Dressler A., 1992, AJ, 103, 1047
Soifer B. T. et al., 1984, ApJ, 278, L71
Solomon P. M., Downes D., Radford S. J. E., 1992, ApJ, 398L, 29
Tacconi L. J., Genzel R., Lutz D., Rigopoulou D., Baker A. J., Iserlohe C., Tecza M., 2002, ApJ, 580, 73
Tanaka I., Yamada T., Aragon-Salamanca A., Kodama T., Miyaji T., Ohta K., Arimoto N., 2000, ApJ, 528, 123
Verma A., Rowan-Robinson M., McMahon R., Efstathiou A., 2002, MNRAS, 335, 574
Wilman R. J., Fabian A. C., Crawford C. S., Cutri R. M., 2003, MNRAS, 338, L19
Wold M., Lacy M., Lilje P. B., Serjeant S., 2000, MNRAS, 316, 267
Wold M., Lacy M., Lilje P. B., Serjeant S., 2001, MNRAS, 323, 231
Wold M., Lacy M., Dahle H., Lilje P. B., Ridgway S. E., 2002, MNRAS, 335, 1017
Yee H. K. C., Ellingson E., 1993, ApJ, 411, 43
Yee H. K. C., Green R., 1987, ApJ, 319, 28
Yee H. K. C., Lopez-Cruz O., 1999, AJ, 117, 1985
Zirbel E., 1997, ApJ, 476, 489

This paper has been typeset from a TEX/LATEX file prepared by the author.